Steel and Composite Structures, *Vol. 22, No. 2 (2016) 235-255*
DOI: http://dx.doi.org/10.12989/scs.2016.22.2.235

Experimental studies on steel frame structures of traditional-style buildings

Jianyang Xue [a] and Liangjie Qi [*]

School of Civil Engineering, Xi'an University of Architecture and Technology, Xi'an, P.R. China

(*Received May 21, 2016, Revised August 13, 2016, Accepted September 29, 2016*)

Abstract. This paper experimentally investigated the behavior of steel frame structures of traditional-style buildings subjected to combined constant axial load and reversed lateral cyclic loading conditions. The low cyclic reversed loading test was carried out on a 1/2 model of a traditional-style steel frame. The failure process and failure mode of the structure were observed. The mechanical behaviors of the steel frame, including hysteretic behaviors, order of plastic hinges, load-displacement curve, characteristic loads and corresponding displacements, ductility, energy dissipation capacity, and stiffness degradation were analyzed. Test results showed that the Dou-Gong component (a special construct in traditional-style buildings) in steel frame structures acted as the first seismic line under the action of horizontal loads, the plastic hinges at the beam end developed sufficiently and satisfied the Chinese Seismic Design Principle of "strong columns-weak beams, strong joints-weak members". The pinching phenomenon of hysteretic loops occurred and it changed into Z-shape, indicating shear-slip property. The stiffness degradation of the structure was significant at the early stage of the loading. When failure, the ultimate elastic-plastic interlayer displacement angle was 1/20, which indicated high collapse resistance capacity of the steel frame. Furthermore, the finite element analysis was conducted to simulate the behavior of traditional-style frame structure. Test results agreed well with the results of the finite element analysis.

Keywords: traditional-style buildings; steel frame structure; quasi-static test; mechanical behavior; finite element analysis

1. Introduction

Chinese ancient architecture, with its long history and glorious achievements, formed a unique structural system and has an important influence on architecture of many countries such as Japan, South Korea, the United States, etc. Thus, Chinese ancient architecture has a high value in terms of history, culture, art and science. There are some differences among Chinese ancient architecture, western ancient buildings and modern architectures regarding to building materials and building structures, resulting in significant differences of force transmission mechanism and structural seismic performance. Fig. 1 illustrates a typical ancient wood palace in China. It is characterized by timber-frame structural system, which constitutes the major load-bearing component under seismic excitations. The lateral load-bearing structures and exterior protected construction (such as infilled wall) are divided by their own functions. Therefore, Chinese ancient buildings have the

*Corresponding author, Ph.D. Candidate, E-mail: qiliangjie@gmail.com
[a] Professor, Ph.D., E-mail: jianyang_xue@163.com

http://www.techno-press.org/?journal=scs&subpage=6 ISSN: 1229-9367 (Print), 1598-6233 (Online)

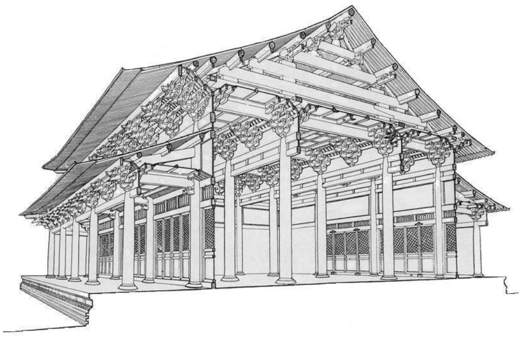

Fig. 1 Ancient wood palace

Fig. 2 Traditional-style buildings

characteristics of “A wall fall down, while the house won’t collapse”.

Previous studies showed that the earliest ancient architecture being found appeared more than 5000 years ago. The first book about the construction of ancient wood structure was published in the Song Dynasty (Zhang *et al*. 2011), and investigations about wood structures began in the 1970s (Liang 1984). As time goes on, the damage of Chinese ancient buildings has increased seriously, and as a result, quite a few have been completely preserved. Wood structures are vulnerable to fire, and are difficult to be used for large and complex buildings.

In order to inherit the precious cultural heritage, the idea of traditional-style buildings constructed with modern construction materials has been raised. Traditional-style buildings combine the appearance of ancient architecture and modern building technology. In recent years, traditional-style buildings are widely used in some cultural and historical cities. Their appearance and construction are significantly different from modern steel frame structures. Fig. 2 shows an example of traditional-style buildings.

In traditional-style buildings, the cornices are especially large, therefore it forms a “Big Roof”. Dou-Gong component, a special construct in the ancient buildings, located between the pillar head and upper surface of the house to prop up a beam and pick up the eaves, is the connection between upper and lower components and used to transfer compressive and tensile stress. Besides, it also plays a decorative role. The square board is called Dou (Fig. 5; D1-D8), the short bow part is named as Gong (Fig. 5; G1-G5). Under earthquakes, Dou-Gong performs a plastic deformation and absorbs seismic energy. Column components, according to different locations, are divided into three types including eave column, short column, hypostyle column and are mostly represented by the form of circular cross section (Fang *et al*. 2011). E-component and Fang-component, connecting elements between two columns, are characterized by rectangular cross-sections (Fig. 5; L2, L4, etc.). They are used as beams so as to transfer horizontal forces. To achieve large space, short column components are usually located above E-component and Fang-component (Zhao *et al*. 2011). Besides, steel is the most commonly used material. There are several examples of traditional-style buildings such as Danfeng Gate of Daming Palace, Luoyang City of Tang Dynasty, DingDing Remnants Museum and so on.

Archaized steel structures, combining characteristics of ancient structures and modern engineering, had the advantages of light weight and high bearing capacity. Also, this type of structure changed the wood mechanical characteristics, absorbing the essence of Chinese ancient architecture. However, some traditional-style steel buildings were destroyed when subject to the earthquake. Take Wuchan Palace in Taiwan as an example, it was located close to the earthquake jgrnskd

(a) Collapse of the whole building (b) Rupture failure of columns

Fig. 3 Seismic damage photos of Wuchang Palace

epicenter. Affected by the 921 chi-chi earthquake, the entire palace building collapsed and the frame structures was only consist of one and a half story after the earthquake while it was made of three stories originally. The seismic damage photos of Wuchang Palace were shown in Fig. 3.

Most researches on the traditional-style buildings used wood materials (Gattesco and Boem 2015, Kouris and Kappos 2014, Parisi and Piazza 2015, Chun *et al*. 2011, Li *et al*. 2015). However, seismic analysis of the traditional-style steel buildings was only experimentally studied in China. Wu (2010) studied the structural composition and mechanical properties of DingDing Remnants Museum steel gates at Luoyang City of Sui and Tang dynasties. The results showed that the gate tower was in a good seismic performance under the earthquake with a magnitude of 7 degrees, and that its performance was affected by the construction sequence. Xue *et al*. (2016c) conducted the seismic experimental researches of the connection between square steel tube column and circular steel tube in the traditional-style buildings. The study showed that the failure was mainly due to the local buckling and welding cracking of rectangular steel tube column flange around the roots. The axial compression ratio, steel yield strength and width-to-thickness ratio had an important influence on bearing capacity, ductility and the stiffness. Ma (2015) performed another research regarding to the inner joints with Dou-Gong components in the traditional-style buildings. It showed a good seismic performance of column-beam core zone with Dou-Gong, and also illustrated that the failure mode was the occurrence of weld cracking at the root of Lu dou's flanges and webs, which was due to the constraint effect of stiffening rings. Xue *et al*. (2015) conducted the cyclic reversed test on the double beam-column joints in traditional steel structures. The experiment results showed that three core zones, including upper, middle and lower core zone, were formed in the traditional inner joints during the loading. The deformation mainly occurred in the lower core zone, and the rupture of beam-column welding joints had a significant influence on the ductility factor.

The above studies were mainly focused on the behaviors of beam-column connections in the traditional steel structures. Few studies have been done on the mechanical behavior and seismic performance of the integrated steel frame structures owing to the special style of traditional-style buildings. Because of the lack of theoretical support and test analysis, the traditional-style steel frame structures can only be designed based on experience and related immature regulations, and it is difficult to guarantee the reliability of the structure. This paper took a scenic hall building as the prototype, and conducted an experimental study on a one-storey and two-bay steel frame structure of traditional-style under low cyclic reversed test. The loading procedure and test setup were

Fig. 4 Steel frame model

introduced. Then the mechanical behaviors of the steel frame, including hysteretic behaviors, order of plastic hinges, load-displacement curve, characteristic loads and corresponding displacements, ductility, energy dissipation capacity, stiffness degradation and strength degeneration were analyzed in detail. A finite element analysis was also conducted and the analytical results were in a good agreement with the experiment results. Test results showed that the Dou-Gong component in steel frame structures acted as the first seismic line under the action of horizontal loads, the plastic hinges at the beam end developed sufficiently and satisfied the Chinese Seismic Design Principle of "strong columns-weak beams, strong joints-weak members". As a result, the welding intensity should be strengthened in the actual project. Moreover, this research could provide references for engineering application and seismic design of traditional-style buildings.

2. Experimental programme

2.1 Test specimen

The experiment was considered to be located in the region with seismic design intensity of 8 degrees, which the corresponding design basic acceleration of ground motion is 2 m/s^2 (0.2 g) and the rare earthquake acceleration is 4 m/s^2 (0.4 g) accordingly. According to the existing design documentation, the specimen was extracted from a steel framed structure of traditional-style building in Xi'an of China and fabricated strictly on the basis of the Building Standards of the Song Dynasty (A.D960-1279) (Li 1100). Keeping the main features unchanged, the two-bay and one-storey steel frame structure of traditional architectural style was then made as a half-scale model. And the specimen, as shown in Fig. 4, had the same characteristics with ancient architectures, including sloping roof, circular columns, and a large space. In addition a simplified welded Dou-Gong component was used in steel frame structures to simulate the Dou-Gong component of mortise-tenon connection in traditional wood structures. The specific size of the specimen is shown in Fig. 5 and the section size of the structural member is in Table 1. Among them, Z1-1, Z1-2 and Z2 column components were divided into two parts, named upper columns (U) and lower columns (L). The upper columns had a rectangular shape while circular steel tubes were adopted for the lower columns. Fig. 6 shows the connection diagrams of upper columns and lower columns. The upper rectangular column was inserted into the lower circular steel tube columns of Z1-1 and Z1-2 with a length of 270 mm. And the upper column Z2U was inserted into the lower column Z2L and extended to the beam bottom flange. In addition, four welding vertical stiffening ribs were put up around the bottom of the upper rectangular steel tube so as to ensure the stability of the connection and the clarity of force transmission; What's more, an inner plate of thickness 5 mm was welded at the height of the beam bottom flange (Fig. 6). The specimen adopted integrity welding technology to provide a better rigidity and stability, and the steel applied to the experiment was Q235B with nominal yield strength of 235 MPa, the thickness of steel were 3 mm, 5 mm, 6 mm, and 10 mm, respectively. The samples of material test were consistent with the corresponding base materials. All the tested materials were taken according to "steel and steel products-location and preparation of test pieces for mechanical testing (GB/T2975-1998)." The thicknesses of these components were measured by vernier calipers. The yield strength, ultimate strength, yield strain, ultimate strain and elastic modulus were measured according to "Metallic materials-tensile testing at ambient temperature (GB/T 228-2002)". The mechanical properties of steel are shown in Table 2.

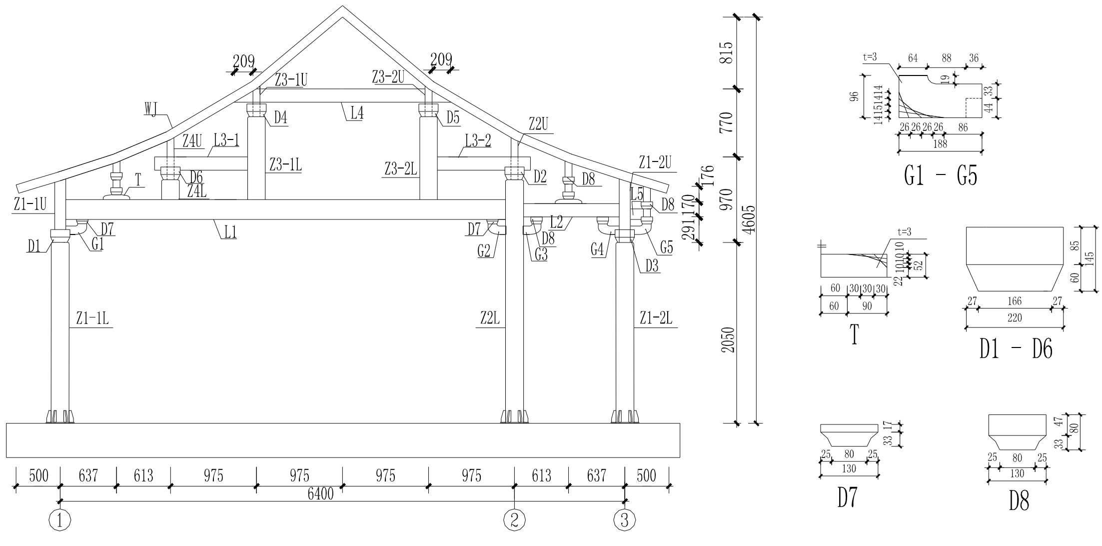

Fig. 5 Dimensions and details of specimen

Table 1 Sizes of components

Components	Control numbers	Section
Columns	Z1-1L, Z1-2L, Z2L	φ203×6
	Z1-1U, Z1-2U	□125×5
	Z3-1L, Z3-2L, Z4L	□125×3
	Z2U, Z4U, Z3-1U, Z3-2U	□80×3
Beams	L1	□225×125×3
	L2, L3-1, L3-2, L4	□150×100×3
	L5	□120×100×3
Roof truss	WJ	□100×3

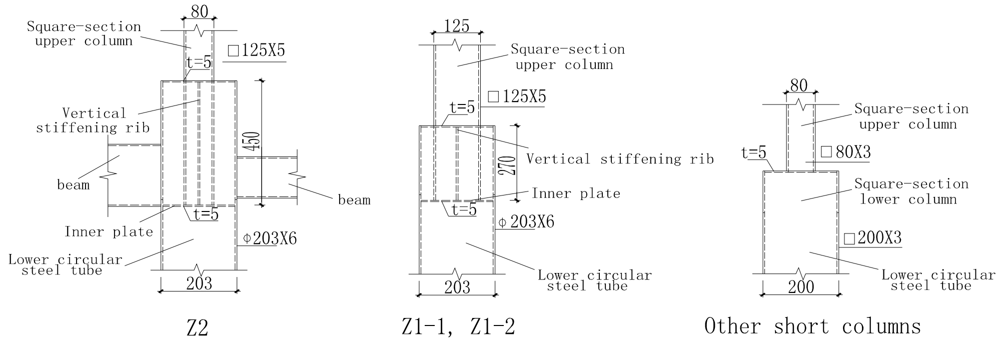

Fig. 6 Connection between upper column and lower column

Table 2 Mechanical properties of steel

Materials	Thickness t (mm)	Yield strength f_y (MPa)	Yield strain ε_y (10^{-6})	Ultimate strength f_u (MPa)	Ultimate strain ε_y (10^{-6})	Elastic modulus E_s (MPa)	Elongation index δ (%)
Plates	3	327.3	1544	476.8	2249	2.12×10^5	21.1
	5	317.6	1557	390.7	1915	2.04×10^5	20.8
	10	289.2	1530	407.1	2154	1.89×10^5	27.8
Tubes	3	335.9	1592	502.4	2381	2.11×10^5	25.6
	6	306.3	1612	362.6	1908	1.90×10^5	25.6

2.2 Measurement and data acquisition devices

The frame structure was instrumented with linear variable differential transducers (LVDTs) at different elevation to monitor the lateral displacements. The dial indicators were installed to monitor the lateral slip of the concrete foundation. On the basis of lateral slip value, the lateral displacement of different components of the specimen could be modified (Ma *et al*. 2015). The arrangement of displacement measuring points is shown in Fig. 7(a). The strains at the beam-end, column-end, Dou-Gong and joint core areas were measured by strain gauges and strain rosettes, respectively. The prefix letters of different gauges have different meanings, for instance, L, Z, Dou and Gong represents beams, columns, Dou component and Gong component, respectively. Besides, displacements and strain data were measured by the automatic intelligent signal acquisition instrument TDS-602, and the arrangement of main strain measuring points is illustrated in Fig. 7(b). One linear variable differential transducer (LVDT1) was installed along the central line of the loading cross-section to monitor the in-plane lateral displacement of the load point of the steel frame. Other LVDTs were also installed to monitor the displacement at the different elevation of the specimen.

2.3 Test setup and procedure

The cyclic loading test was carried out by using a multi-functional electro-hydraulic servo test machine in the Key Laboratory of Structural Engineering at Xi'an University of Architecture and

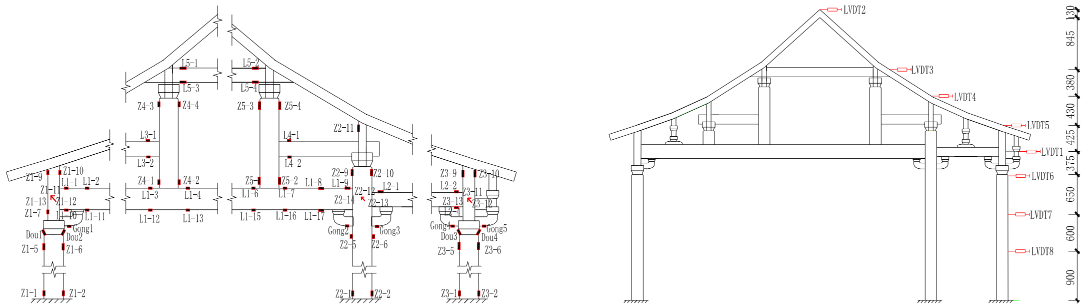

(a) Distribution of strain gauges (b) Layout of displacement transducers

Fig. 7 Arrangement of measuring points

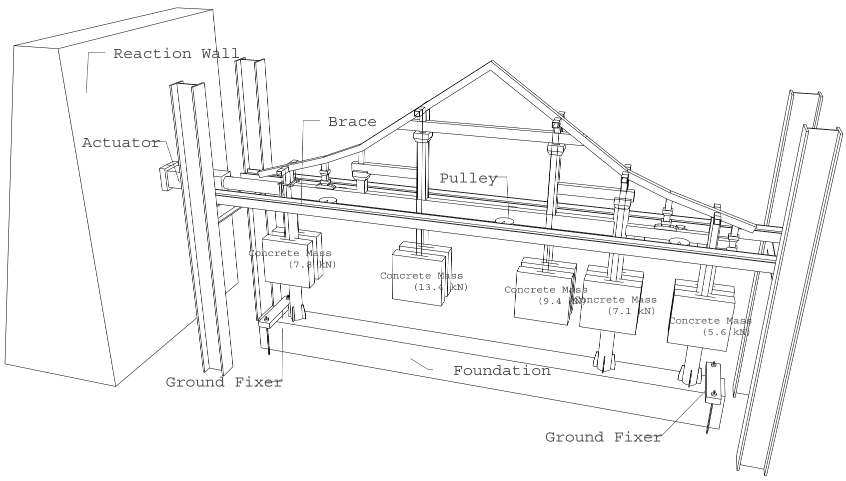

Fig. 8 Test setup

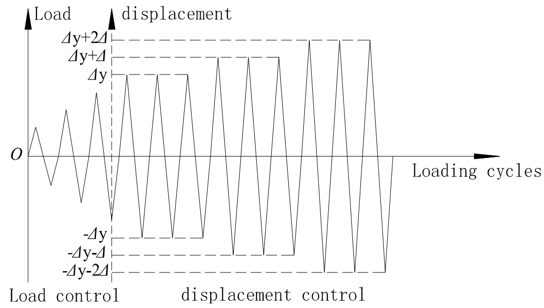

Fig. 9 Loading procedure

Technology, China. The test setup is shown in Fig. 8. The column base of the specimen was embedded in the concrete foundation, which in turn was restrained by two strong steel beams to prevent the frame specimen from lifting during testing (Wang *et al*. 2016). The brace pulleys were adopted on both sides of the frame planes so as to ensure that the frame was stable during the loading process. Firstly, based on the real surface load condition, the vertical weights of 7.8 kN, 13.4 kN, 9.4 kN, 7.1 kN and 5.6 kN were imposed on the top of frame columns (i.e., Z1-1, Z3-1, Z3-2, Z2 and Z1-2, respectively). With the suspension of concrete masses, the lateral load was applied by imposing cyclically lateral varying displacements at the height of the girder by a 500 kN capacity bi-directional hydraulic actuator. The loading procedure was illustrated in Fig. 9 which involved two loading steps, named a load-controlled step and a displacement-controlled step. These steps were divided by yielding of the structures, and the horizontal loads linearly changed from 0 kN to 140 kN with an interval of 20 kN once a time. Afterward, some damage evolution occurred and the specimen went into the plastic stage. The increment of the displacement was denoted as the yield displacement Δ_y, and each displacement-loading step was repeated three times in increments of 10 mm until a significant decline in the loading-displacement loop was observed or the displacement reached a specific value that the specimen is unable to bear it. During the loading procedure, the data were recorded automatically by a computer.

3. Results and discussion

3.1 Damage evolution and failure modes

The observations of the experiment are described as follows. The electro-hydraulic servo actuator was applied to the reciprocating load during the experiment, and the loading direction was defined as positive and negative for the convenience of description.

In the early loading stage of horizontal load, the force was adopted primarily as the load-controlled step, and the strain at each area was not significant, in addition, there was a linear relationship between horizontal loads and displacements, which meant the whole frame was still in elastic stage. When the load added to -90 kN, the right bottom region of Dong D1 yielded at first; the strain of Gong G2 reached yield strain after the lateral load reached -100 kN; vertical cracks occurred at the northwest corner of Gong G4 until the horizontal load reached ±140 kN.

Then displacement-controlled method was applied subsequently. Fig. 10 shows the failure modes of the specimen under cyclic loading. The welding crack at the bottom flange of Gong G4 was 25 mm when the cyclic loading of displacement was ±55 mm (Fig. 10(a)), the concave deformation occurred at Gong G3 and the crack of welding appeared; when the cyclic loading was ±85 mm, weld cracking occurred at the connected location between Gong G1, Dou D1 and the joint region at the bottom of the column Z1 and Dou D1, then cracks about 5 mm occurred approximately, followed by outside-plane convex deformation and weld fracture at column Z1-2 (Fig. 10(b)), tearing of welds at right ends of beam L2 turned up, crack penetration showed up at the right bottom flange end of beam L1; when the displacement added up to ±115 mm, the crack extended to the upper region at the junction of Gong G1 and Dou D1, and left bottom flange of beam L2 showed a weld fracture penetrably; the convex deformation of the northwest corner at column Z1 occurred after the lateral displacement reached +125 mm, the shear failure appeared at the right side of beam L1 (Fig. 10(c)), and the left sides of beam L5 disconnected completely. What's more, a serious shear deformation occurred at Dou D2 (Fig. 10(d)).

According to the test observation and the measured strain data, the failure characteristics of the steel frame structures of traditional-style buildings are as follows.

(1) Whether positive or negative loading, the first two regions which reached yield strain were at the strain gauges of Dou1 and Gong2, and thus the earliest plastic hinge occurred.

(a) Crack of 25mm at Gong G4

(b) Weld fracture at upper column Z1-2

(c) Shear failure at column Z1-1

(d) Shear deformation of Dou D2

(e) Rupture at the lower flange of beam L1

(f) Tensile failure of left side of beam L2

(g) Tearing of Gong G4

(h) Destruction at the end of beam L1

Fig. 10 Failure modes of specimens

(2) The plastic hinge at the beam end developed sufficiently, and convex deformation showed up at the left end of the beam L1, tearing occurred between steel web and flange, which is shown in Fig. 10(e); breaking appeared at both ends of beam L2 (Fig. 10(f)), which was mainly because Dou-Gong component destructed at first, and then bending moment at the beam end increased, tearing appeared along the interface of the web and flange of Gong G2, G3 and G4 along the horizontal direction (Fig. 10(g)). In addition, shear deformation was obvious at Dou D2, indicating that the shear effect was significant under the action of horizontal load.

(3) The horizontal shear failure appeared at the loading end of Z1 which was mainly because the stiffness of plate stiffener was stronger than that of the 3 mm steel plate. With the increasing of external loading, excessive shear was formed on the column Z1-1.

(4) Compared with the beam and Dou-Gong components, no failure occurred obviously at column bottom, the time of reaching yield strain of column bottom was later than that of beam end. Dou-Gong component first destroyed under the action of horizontal loads, followed by beam ends (Fig. 10(h)), and the plastic hinge was formed at the column end at last. At the end of the loading process, the core areas of joints didn't yield. From the above description, steel frames of traditional-style could meet the requirements of the seismic design of "strong columns-weak beams, strong joints-weak members".

3.2 Plastic hinge

The plastic hinge position and different forming orders of plastic hinge will cause different failure modes in the frame structure. From the strain value measured by different strain gauges and macro phenomenon (such as local buckling, deformation and so on), the plastic hinge region can be determined (Liu *et al*. 2014). The sequence and positions of plastic hinges in the steel frame structure of traditional-style are shown in Fig. 11, and the final structural deformation of the frame is shown in Fig. 12.

Test results showed that multiple seismic lines were formed under the action of horizontal force, and first plastic hinge occurred at Dou-Gong component, which serves as the main component of the anti-seismic line. It was the first to resist the impact of the horizontal earthquake action. Subsequently, the plastic hinge appeared at the beam end of the structure, and seismic energy was consumed by beam deformations, which acted as the second anti-seismic line to protect the security of columns and floors in this structure.

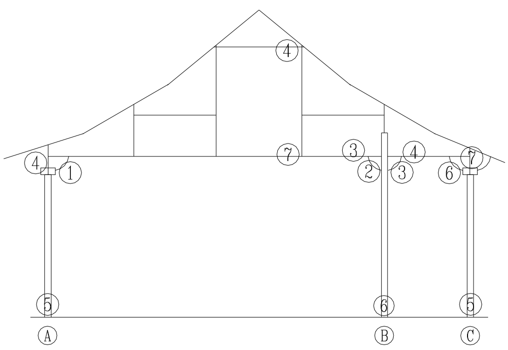

Fig. 11 Subsequence of plastic hinges of frame

Fig. 12 Structural deformation

3.3 Hysteretic behaviors

The hysteresis loop and force-displacement response envelope reflect the relationship between load and deformation of the overall structure comprehensively (Xue *et al.* 2016a). The hysteresis curve of the specimen is shown in Fig. 13, P and Δ represent horizontal load and horizontal displacement of structural girder, respectively. The hysteresis curve of traditional-style steel frame structure has the following characteristics:

(1) In the initial loading stage, hysteresis curve cycled along a straight line basically, there was a linear relationship between load and displacement, no obvious stiffness degradation occurred, and residual deformation was negligible during the unloading stage.
(2) With the increase of load, Dou and Gong components gradually yielded and the slope of the hysteresis curve changed. Besides, surrounding area of hysteresis loops was increasing. When unloading to zero, an obvious residual deformation was observed, and it meant structure entered the stage of nonlinear working.
(3) After yielding of the frame structures, cracking appeared at the web and flange of Gong component under horizontal load, tearing and rupture showed up at the upper flange of Dou components, plastic deformation aggravated, the bearing capacity and stiffness

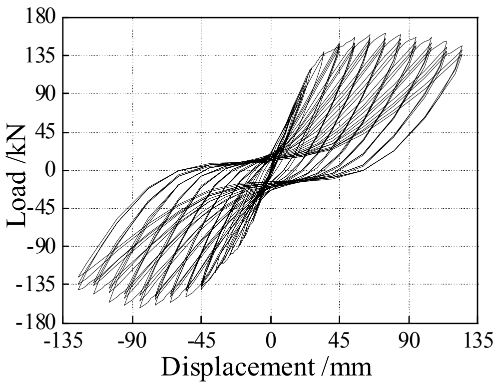

Fig. 13 Hysteresis curve

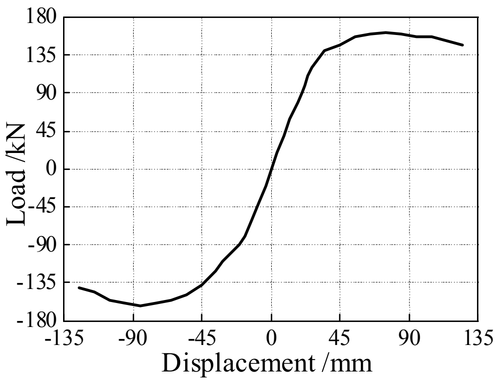

Fig. 14 Force-displacement response envelope

(4) owing to the influence of the cumulative damage of the specimens, hysteresis loop turned into anti-S shaped slightly, a certain pinching phenomenon occurred. With the increment of lateral load, plastic hinges occurred at the beam end. Convex deformation and tearing occurred at the web and flange of beam end, then the beam end destroyed, resulting in the increasing of disconnected crack gap and the change of local structural system. Besides, pinching phenomenon aggravated in hysteresis loops and the curve changed into Z-shape.
(5) The hysteresis loops showed some differences with the conventional steel structures which were plump in general

3.4 Force-displacement response envelope

Force-displacement response envelope is an important indicator for the seismic design of structures or component for the reason that they reveal the mutual relationship between lateral loads and the corresponding displacement under lateral load (Han *et al*. 2007). The force-displacement response envelope of the tested steel frame is shown in Fig. 14. It can be seen from the figure that the steel frame structures in traditional-style could be divided into three stages, i.e. the elastic stage, plastic stage and failure stage. During the elastic phase, structure stiffness remained unchanged basically. When loading up to the yield point, Dou-Gong component gradually yielded, the stiffness of the whole specimen decreased correspondingly. After reaching the peak load point, load decreased and the force-displacement response envelope declined more gently which demonstrated the structure had a good deformation ability and good ductility. The force-displacement response envelope was not symmetrical completely owing to the asymmetry of structural form.

3.5 Characteristic values

The characteristic loads (i.e., yield load, peak load and ultimate load), corresponding with characteristic displacement and ductility factors are listed in Table 3. P_y stands for the yield load, which was confirmed by the method of universal yield moment (Lubliner 2006, Xue *et al*. 2016b). The calculating process is shown in Fig. 15. P_m and P_u stand for the peak load and ultimate load, respectively, which were obtained from the test results. When a significant decline in the loading-displacement loop was observed or the displacement reached a specific value that the specimen is unable to bear it, the test could be stopped. As for this test, the ultimate displacement angle reached approximately 1/20 and the specimen could not bear a greater displacement. Then for the safety of the experiment, the ultimate displacement was confirmed accordingly. Δ_y, Δ_m and Δ_u are the displacements corresponding to the load P_y, P_m and P_u, respectively. θ_y, θ_m and θ_u are the inter-storey drift angles corresponding to the load P_y, P_m and P_u. The inter-storey angles are defined as $\theta_{\mathrm{i}} = \Delta_i / H$, where Δ_i stands for the inter-storey displacement, H stands for the height of the girder of the structure. Displacement ductility is an important performance index for structure, which can reflect if the structure has an excellent plastic deformation capacity. Ductility factors are usually represented by ductility coefficient, which is defined as $\mu = \Delta_u / \Delta_y$.

In the case of rare earthquake, according to Chinese Seismic Design Code (GB50011-2010), the elastic plastic layer displacement angle should be less than a specified limit value (1/50 of steel frame structure) in order to prevent the collapse of the structure. Table 3 demonstrates the maximum horizontal displacement of the steel frame at the height of the girder and the ultimate displacement angle reached 1/20 at the failure load point, which exceeded the aforementioned displacement limits of 1/50, indicating that the experimental steel frame structure in traditional-style building had a strong capacity to resist progressive collapse. Besides, the positive displacement angle of the structure was always smaller than that of the negative direction in the early loading stage, which was owing to the asymmetric arrangement of the structural members.

The overall displacement ductility factors of the specimen were 3.26 and 2.74 in the positive and negative directions, respectively. The ductility coefficient was a little smaller than general situation (Park *et al*. 2007, Shafaei *et al*. 2014, Sun *et al*. 2011) for the reason that horizontal shear destruction of Dou-Gong component occurred as the load increase, and that weld fracture or steel rupture appeared at the beam end due to large bending moment, which reduced the bearing capacity of the structure.

3.6 Energy dissipation capacity

The area of hysteresis loops (i.e., Total energy consumption) reflects the energy dissipation capacity of structures to a certain extent which also indicates their seismic performance. The energy dissipation ratio E and equivalent viscous damping coefficient h_e are important indexes using to quantify the energy dissipation capacity of structures and members. The energy dissipation ratio E and equivalent viscous damping ratio h_e were calculated using Eqs. (1)-(2) to evaluate the accurate energy dissipation ability of the specimens. $S_{(\mathrm{ABC+CDA})}$ is the area of the shadow and $S_{(\mathrm{OBE+ODF})}$ is represented by the sum of the area of the triangle OBE and triangle ODF as shown in Fig. 16.

$$E = S_{(\mathrm{ABC+CDA})} / S_{(\mathrm{OBE+ODF})} \tag{1}$$

$$h_{\mathrm{e}} = E / 2\pi \tag{2}$$

Table 3 Characteristic values

Loading direction	Yield point			Peak point			Failure point			Ductility factor μ
	P_y (kN)	Δ_y (mm)	θ_y	P_m (kN)	Δ_m (mm)	θ_m	P_u (kN)	Δ_u (mm)	θ_u	
Positive	142.24	38.32	1/66	161.55	75	1/34	147.14	124.99	1/20	3.26
Negative	138.45	45.58	1/56	161.67	85	1/30	141.34	124.98	1/20	2.74

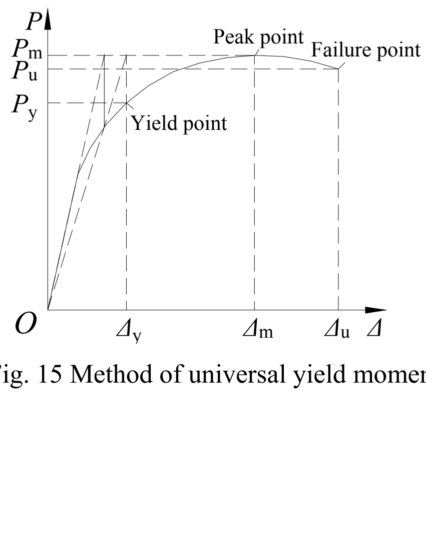

Fig. 15 Method of universal yield moment

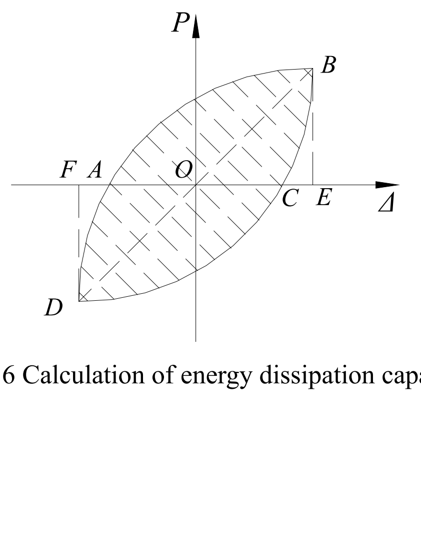

Fig. 16 Calculation of energy dissipation capacity

Table 4 Energy dissipation of specimen

Feature point	Yield point	Peak point	Failure point
Total Energy consumption /(kN·mm^{-1})	3204.02	6671.99	9281.36
Energy dissipation ratio E	0.49	0.58	0.53
Equivalent viscous damping coefficient h_e	0.078	0.092	0.084

Total Energy consumption, energy dissipation ratio E, equivalent viscous damping coefficient he at different feature points are shown in Table 4. The data in the table shows that as the load increased, the area of hysteresis loops increased gradually and the total energy consumption increased accordingly. However, energy dissipation ratio E of the specimen showed a decreasing trend after the first increase, which reached peak at the peak point of bearing capacity. The key reason was that failure of Dou-Gong components occurred near the peak point of the structure, and that crack gap increased after fracture of beam L1 and L2, thus the local structural system changed and the energy dissipation ability dropped as well. Moreover, the area of hysteresis loops decreased because of the pinching phenomenon, and the area of $S_{(ABC+CDA)}$ at specific point (i.e., failure point) in Fig. 16 decreased as well while the area of $S_{(\Delta OBE+\Delta ODF)}$ was still increasing.

3.7 Stiffness degradation

Stiffness of test specimens under low cyclic reversed loading can be expressed by secant stiffness which is defined as the ratio of load and the corresponding displacement in each loop of positive or negative direction (Xu *et al*. 2016). Stiffness decreased with the increase of cycle, which is called stiffness degradation. Based on the overall equivalent stiffness $K = P / \Delta$, it is used to measure the degree of stiffness degradation. Fig. 17 illustrates the stiffness degradation rule of traditional-style construction steel frame structure, it can be seen from the Fig. 17 that the initial stiffness of the specimen showed differences in positive and negative directions to a certain extent. The stiffness degradation in negative was faster than that of positive stiffness degradation, which was mainly caused by the asymmetric arrangement of structure component; With the repeated load applied to the frame, the stiffness of both directions were approaching; Stiffness degraded faster in early stage, plastic development and stiffness attenuation slowed down with the structural damage accumulation.

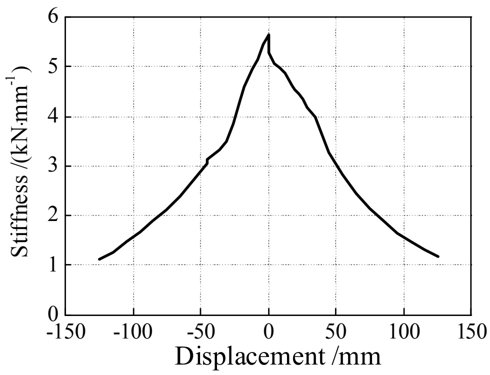

Fig. 17 Stiffness degradation

Table 5 Coefficients of Strength degeneration

λ_i	δ_y	$3\delta_y$	$5\delta_y$	$7\delta_y$	$9\delta_y$
Positive	1.103	0.950	0.932	0.928	0.921
Negative	0.956	0.935	0.915	0.891	0.890

3.8 Strength degeneration

After entering the plastic state, in the case of constant displacement amplitude, the bearing capacity of structural members will decrease with the increase of the cycles of repeated loading. The degradation of the strength can be expressed by the coefficients of the strength degeneration. It is characterized by the ratio of the peak load of third-cycle loading to that of first-cycle loading, named λ_{i}, and the different coefficient of strength degeneration under different levels of loading is shown in Table 5.

It can be seen from the table that the strength degradation trends of the specimen in the positive and negative direction were basically the same. In the early period of displacement-controlled stage, the degeneration degree was more significant than that of the terminal stage. In the loading stage of δ_y – $5\delta_y$, the degradation of bearing capacity of the specimen was 15.5% and 4.3% respectively in the positive and negative direction, and the bearing capacity of the specimen was degraded by 1.2% and 2.7% in positive and negative direction respectively during the loading period of $5\delta_y$ – $9\delta_y$. The reasons were the failure of major members (shear deformation of Dou-Gong, rupture of the beam end) in traditional-style steel frame occurred in the early stage of displacement-controlled period. However, the displacement increased continually due to the failure of the main components at the later loading stage, the strength didn't decrease significantly. Even at the end of the test, the bearing capacity of the specimen was also close to 0.9, which showed that the stability of bearing capacity of traditional-style steel frame structure was very good and the strength could not decrease sharply.

3.9Strain distribution

Because of the existing of special members, such as Dou-Gong component, the mechanical mechanism subjected to earthquake shows some difference compared with regular steel frames. The strain distribution at different locations was illustrated in Fig. 18.

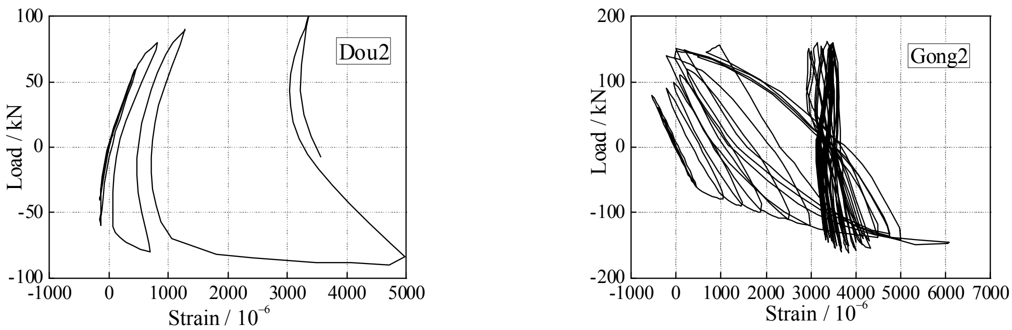

Fig. 18 Hysteretic loops of load versus strain

It can be found from the figure that the load-strain curve showed a linear increase in the early stage of loading, which indicated it was in the elastic stress stage; When the load increased to 90 kN, the strain of Dou-component increased suddenly and exceeded the yield strain. Subsequently, Gong component yielded before the test specimen entered the plastic loading stage. However, no obvious yield phenomenon appeared at the core zone of the joints and column end. It is illustrated that the strain distribution is reasonable in traditional-style buildings and it has excellent seismic performance.

4. Finite element analysis

4.1 Traditional-style steel frame modeling

Pushover analysis is more convenient to determine the target displacement and bearing capacity under different earthquakes (Zhou *et al*. 2015). By using finite element software Abaqus to establish the three-dimensional model of the specimen, the Pushover analysis was conducted. The whole specimen model is shown in Fig. 19. Thin shell element was chosen to calculate the structure modeling, and the ideal elastic-plastic hardening model was used as the steel material regulation, also, keeping consistent boundary conditions with the experiment. The stress-strain curve of steel used in the analysis was represented in Fig. 20, it is mathematically expressed as Eq. (3). E stands for elasticity modulus, E_p represents the slope of the stress - strain relationship in the elastic-plastic stage. σ_y and σ_u stand for yield strength and peak strength, respectively, ε_u represent the strain corresponding to σ_u. They have been implemented in the finite element program Abaqus and all these indexes were obtained from the material tests. The modulus of elasticity (E_s), yield strength (f_y) and ultimate strength (f_u) of steel were shown in Table 2, and the strain corresponding to ultimate stress was defined as 0.08. In addition, the method of fixed connection was applied to the simulation of welds. In order to prevent the stress concentration at the loading end, rigid base plate was set up at the loading position.

$$\sigma = \begin{cases} E \cdot \varepsilon & (\varepsilon \le \varepsilon_y) \\ \sigma_y + E_p \cdot (\varepsilon - \varepsilon_y) & (\varepsilon_y < \varepsilon_y < \varepsilon_u) \\ \sigma_u & (\varepsilon > \varepsilon_u) \end{cases} \tag{3}$$

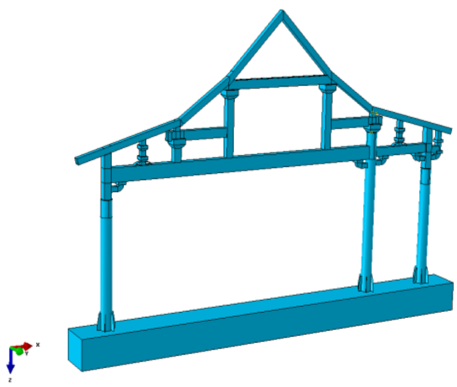

Fig. 19 Finite element model

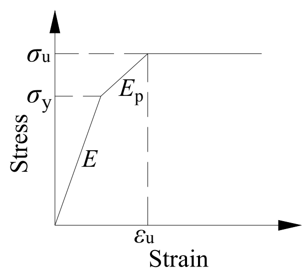

Fig. 20 The idealized stress–strain relationship

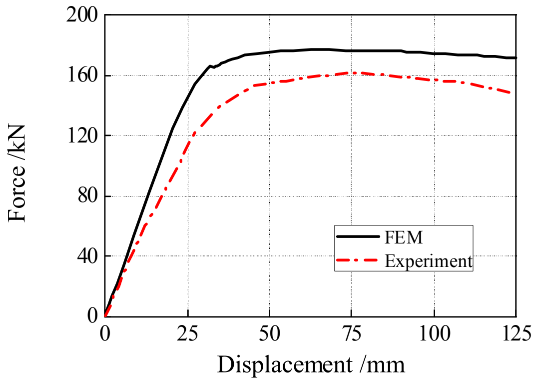

Fig. 21 Comparison of force-displacement response envelopes

Table 6 Results comparison between experiment and FEM

Results	Yield point		Peak point		Failure point	
	P_y (kN)	Δ_y (mm)	P_m (kN)	Δ_m (mm)	P_u (kN)	Δ_u (mm)
Experiment	142.24	38.32	161.55	75	147.14	124.99
FEM	165.31	31.66	176.90	62.45	171.51	125.00
Experiment / FEM	1.16	0.83	1.10	0.83	1.17	1.00

4.2 Numerical results

The finite element analysis method was used to simulate the whole process from yield to the failure of the traditional-style steel frame structures. The calculated results are shown in Fig. 21. The test results and analytical values based on the finite element software are compared in Table 6. From the table, the load and displacement at yield, peak and ultimate points obtained from Abaqus are close to the experimental results. All the FEM load values are larger than the experimental results, while the displacements showed an opposite tendency. The maximum error at the end of test was 16.5% for the reason that it was the structural damage accumulation and stiffness degeneration of the structure which could not be reflected by software.

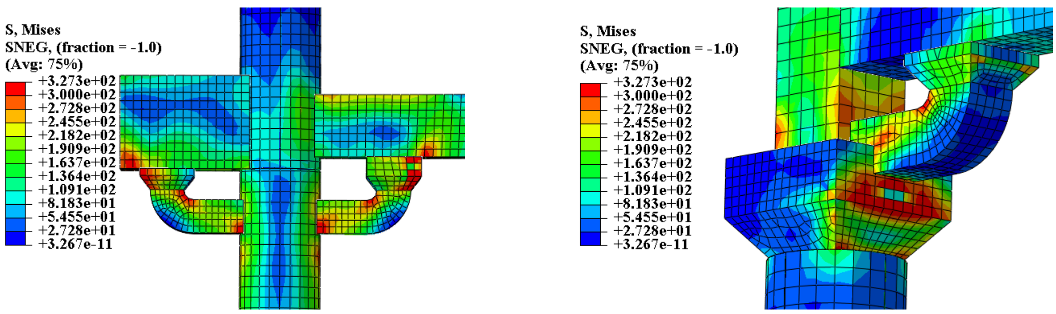

(a) Inner joint on column Z2 (b) Right bottom of D1

Fig. 22 Strain of specific region

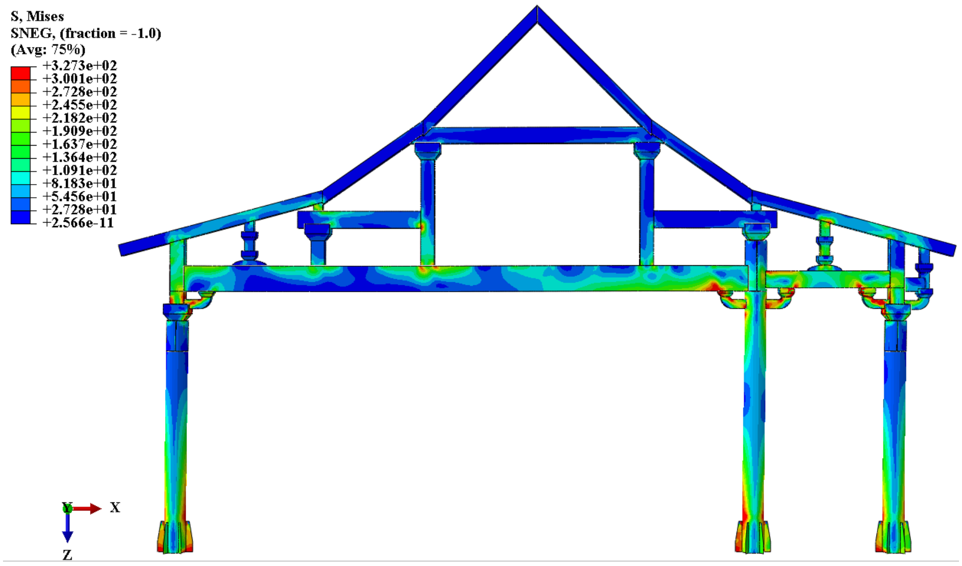

Fig. 23 Strain distribution contours

According to the further calculation, the average value of the ratio of experiment to FEM is 1.014, the standard deviation is 0.141 and variable coefficient is 0.139. There was a consistency between the finite element calculation result and the test result from a general view and they agreed well with each other. Therefore, the finite element modeling can thus be adopted to evaluate the nominal behavior of steel frame structures in traditional-style buildings.

Fig. 22 shows the strain distribution of the inner joint on column Z2 and right bottom region of D1 at the yield point. The right bottom region of D1 yielded firstly during the loading test in the numerical study, following the upper region of G2. The upper region of Gong component achieved the maximum strain values, which demonstrated that it entered the plastic stage. The beam flanges were close to the yield strain while the column end was still in elastic stage, which met the Chinese Seismic Design Requirements of “strong columns and weak beams”.

The strain contours are shown in Fig. 23 at the moment when the specimen was loaded to elastic-plastic layer displacement angle limit value (i.e., 1/50). The study found that the stress at Dou-Gong, eastern sides of L1, and the beam end of L2 was obvious (the red region), which represented the weak parts of the overall steel frame structure. Besides, the stress development of each component was analyzed, Dou-Gong component yielded firstly and played a role as the first seismic line; and then plastic hinges occurred at the end of beam L1 and L2 which demonstrated the aggravated damage of the structure. When the structure was close to the failure load, column end of Z1-1, Z1-2 and Z2 all reached the yield stress, which was consistent with the test results. At the same time, the interlayer displacement angle of the floor exceeded 1/50, which showed that the steel frame structure had a good deformability.

5. Conclusions

The performance of steel frame structures of traditional-style buildings subjected to combined constant axial load and cyclic loading was investigated by the experiment. Experimental results were compared with those of finite element analysis. Both experimental and analytical results are demonstrated as follows:

- The Dou-Gong component of steel frame structure first yielded when loading to -100kN, then tearing along the web and flange junction occurred. As the load increased, plastic hinges at the beam end developed sufficiently, base metal at the beam end destroyed and the failure mode belongs to the beam-hinge mechanism. Hysteresis curve changed into a Z-shape form, which was mainly due to the gap between girder and columns increased after the rupture occurred, the local structural system changed and there were some differences with conventional steel frame structures.
- The integrated structure maintained a high bearing capacity and a strong deformation capacity in the whole process of pseudo static test. The interlayer displacement angle reached 1/20 when the frame destroyed, and the coefficients of strength degeneration were close to 0.9 at the end of the test, which showed an excellent collapse resistant capacity of traditional-style buildings. The energy dissipation ratio was between 0.49-0.58 and it showed a trend of increased first and then decreased.
- The overall displacement ductility factors of the specimen were 3.26 and 2.74 in the positive and negative directions, respectively. The initial stiffness of the test structure had a certain difference in two directions. The negative stiffness degradation was faster than that in positive direction, and the stiffness degradation was more significant in the early stage of loading.
- In the loading stage of $\delta_y - 5\delta_y$, the degradation of bearing capacity of the specimen was 15.5% and 4.3% respectively in the positive and negative direction, and the bearing capacity of the specimen was degraded by 1.2% and 2.7% in positive and negative direction during the loading period of $5\delta_y - 9\delta_y$. The reasons were the failure of most components occurred in the early stage of displacement-controlled period.
- All the FEM load values are larger than the experimental results, while the displacements showed an opposite tendency. The reason was the structural damage accumulation and stiffness degeneration of the structure which could not be reflected by software. The average value of ratio of test to FEM is 1.014 and the standard deviation is only 0.141. Moreover, there was a consistency between the finite element calculation result and the test from a general view and they agreed well with each other.

Acknowledgments

This work was supported by the National Natural Science Foundation of China (Grant no. 51208411) and Technology Research Task of China State Construction Engineering Corporation (Grant no. CSCEC-2012-Z-16). This work presented herein was conducted in the Structural Engineering and Earthquake Resistance Key Laboratory of Chinese Ministry of Education at Xi'an University of Architecture & Technology, which is gratefully acknowledged.

References

Chun, Q., Yue, Z. and Pan, J.W. (2011), "Experimental study on seismic characteristics of typical mortise-tenon joints of Chinese southern traditional timber frame buildings", *Sci. China Technol. Sci.*, **54**(9),

2404-2411.
Fang, D.P., Iwasaki, S., Yu, M.H., Shen, Q.P., Miyamoto, Y. and Hikosaka, H. (2001), "Ancient Chinese timber architecture. I: Experimental study", *J. Struct. Eng.*, **127**(11), 1348-1357.
Gattesco, N. and Boem, I. (2015), "Seismic performances and behavior factor of post-and-beam timber buildings braced with nailed shear walls", *Eng. Struct.*, **100**(1), 674-685.
GB50011-2010 (2010), Code for seismic design of buildings; China Architecture & Building Press, Beijing, China.
Han, L.H., Huo, J.S. and Wang, Y.C. (2007), "Behavior of steel beam to concrete-filled steel tubular column connections after exposure to fire", *J. Struct. Eng.*, **133**(6), 800-814.
Kouris, L.A.S. and Kappos, A.J. (2014), "A practice-oriented model for pushover analysis of a class of timber-framed masonry buildings", *Eng. Struct.*, **75**(15), 489-506.
Li, J. (1100), *Building Standards of the Song Dynasty*, Royal Press, Kaifeng, China.
Li, X.W., Zhao, J.H., Ma, G.W. and Chen, W. (2015), "Experimental study on the seismic performance of a double-span traditional timber frame", *Eng. Struct.*, **98**(1), 141-150.
Liu, Z.Q., Xue, J.Y., Zhao, H.T. and Gao, L. (2014), "Cyclic test for solid steel reinforced concrete frames with special-shaped columns", *Earthq. Struct.*, **7**(3), 317-331.
Liang, S.C. (1984), *A Pictorial History of Chinese Architecture*, MTT Press, Boston, MA, USA.
Lubliner, J. (2006), *Plasticity Theory*, Pearson Education, Upper Saddle River, NJ, USA.
Ma, L.L. (2015), "Experimental study on seismic behavior of eave column joints with Dou-Gong in steel imitated ancient building", Master Dissertation; Xi'an University of Architecture and Technology, Xi'an, China.
Ma, H., Xue, J.Y., Liu, Y.H. and Zhang, X.C. (2015), "Cyclic loading tests and shear strength of steel reinforced recycled concrete short columns", *Eng. Struct.*, **92**(1), 55-68.
Parisi, M.A. and Piazza, M. (2015), "Seismic strengthening and seismic improvement of timber structures", *Constr. Build. Mater.*, **97**(30), 55-65.
Park, H.G., Kwack, J.H., Jeon, S.W., Kim, W.K. and Choi, I.R. (2007), "Framed steel plate wall behavior under cyclic lateral loading", *J. Struct. Eng.*, **133**(3), 378-388.
Shafaei, J., Hosseini, A. and Marefat, M.S. (2014), "Seismic retrofit of external RC beam-column joints by joint enlargement using prestressed steel angles", *Eng. Struct.*, **81**(15), 265-288.
Sun, G.H., He, R.Q., Qiang, G. and Fang, Y.Z. (2011), "Cyclic behavior of partially-restrained steel frame with RC infill walls", *J. Constr. Steel Res.*, **67**(12), 1821-1834.
Wang, F., Su, M.Z., Hong, H., Guo, Y.R. and Li, S.H. (2016), "Cyclic behaviour of Y-shaped eccentrically braced frames fabricated with high-strength steel composite", *J. Constr. Steel Res.*, **120**, 176-187.
Wu, X.Y. (2010), "Mechanical properties of Dingding gate steel structure component", Master Dissertation; Chang'an University, Xi'an, China.
Xu, W., Han, L.H. and Li, W. (2016), "Seismic performance of concrete-encased column base for hexagonal concrete-filled steel tube: Experimental study", *J. Constr. Steel Res.*, **121**, 352-369.
Xue, J.Y., Wu, Z.J., Sui, Y. and Liu, Z.Q. (2015), "Experimental study on seismic performance of steel double-beams column exterior joints in antique style building", *J. Build. Struct.*, **36**(3), 80-89.
Xue, J.Y., Gao, L., Liu, Z.Q., Zhao, H.T. and Chen, Z.P. (2016a), "Experimental study on mechanical performances of lattice steel reinforced concrete inner frame with irregular section columns", *Steel Compos. Struct.*, *Int. J.*, **16**(3), 253-267.
Xue, J.Y., Huang, X.G., Luo, Z. and Gao, L. (2016b), "Experimental and numerical studies on the frame-infill interaction in steel reinforced recycled concrete frames", *Steel Compos. Struct.*, *Int. J.*, **20**(6), 1391-1409.
Xue, J.Y., Zhai, L., Gao, G.W., Dong, J.S., Ge, H.P., Liu, Z.Q. and Wu, K. (2016c), "Experimenta1 study on seismic performances of connections between rectang1ar stee1 pipe column and circu1ar stee1 pipe column in imitated ancient bui1ding", *J. Build. Struct.*, **37**(2), 81-91.
Zhang, X.C., Xue, J.Y., Zhao, H.T. and Sui, Y. (2011), "Experimental study on Chinese ancient timber-frame building by shaking table test", *Struct. Eng. Mech.*, *Int. J.*, **40**(4), 453-469.
Zhao, H.T., Xue, J.Y., Sui, Y. and Xie, Q.F. (2011), *Chinese Ancient Buildings and Corresponding Seismic*

Method, Science Press, Beijing, China.
Zhou, T., Jia, Y.M., Xu, M.Y., Wang, X.D. and Chen, Z.H. (2015), "Experimental study on the seismic performance of L-shaped column composed of concrete-filled steel tubes frame structures", *J. Constr. Steel Res.*, **114**, 77-88.

CC